



## Micro-Opto-Electro-Mechanical Device Based on Flexible $\beta$ -Ga<sub>2</sub>O<sub>3</sub> Micro-Lamellas

Marco Peres,<sup>1,2,z</sup> A. J. S. Fernandes,<sup>3</sup> F. J. Oliveira,<sup>4</sup> L. C. Alves,<sup>5</sup> E. Alves,<sup>1</sup> T. S. Monteiro,<sup>2</sup> S. Cardoso,<sup>2,6</sup> M. Alonso-Orts,<sup>7</sup> E. Nogales,<sup>7</sup> B. Méndez,<sup>7</sup> E. G. Vllora,<sup>8</sup> K. Shimamura,<sup>8</sup> and K. Lorenz<sup>1,2</sup>

<sup>1</sup>IPFN, Instituto Superior Técnico (IST), Campus Tecnológico e Nuclear, P-2695-066 Bobadela LRS, Portugal

<sup>2</sup>Instituto de Engenharia de Sistemas de Computadores-Microsystems and Nanotechnology (INESC-MN), Lisbon, Portugal

<sup>3</sup>IN and Physics Department, University of Aveiro, 3810-193 Aveiro, Portugal

<sup>4</sup>CICECO and Materials and Ceramic Engineering (DEMaC), University of Aveiro, 3810-193 Aveiro, Portugal

<sup>5</sup>C2TN, Instituto Superior Técnico (IST), Campus Tecnológico e Nuclear, P-2695-066 Bobadela LRS, Portugal

<sup>6</sup>Instituto Superior Técnico, Universidade de Lisboa, Lisbon, Portugal

<sup>7</sup>Departamento de Física de Materiales, Universidad Complutense de Madrid, 28040 Madrid, Spain

<sup>8</sup>National Institute for Materials Science, Tsukuba 305-0044, Japan

A thermal actuator based on thin flexible lamellas of Ga<sub>2</sub>O<sub>3</sub> was designed in order to demonstrate the potential of this semiconductor for micro-opto-electro-mechanical applications (MOEMs). The working principle of these devices is based on the thermal expansion that induces a vertical movement resultant of the lamella elongation due the self-heating/Joule effect. Upon excitation with photons, electrons or ions, intrinsic luminescence bands associated with self-trapped excitons and donor-acceptor pair recombination dominate the emission spectrum. When a current passes through the device, simultaneously with the thermal expansion, this luminescence is strongly quenched. Based on systematic Photoluminescence and Raman studies as a function of temperature and as a function of the applied power it is demonstrated that the observed luminescence quenching is directly related with the Joule heating effect. This work presents for the first time a thermal actuator based on Ga<sub>2</sub>O<sub>3</sub> and it intends to be a stimulus for future works on MOEMs applications based on this semiconductor.

© The Author(s) 2019. Published by ECS. This is an open access article distributed under the terms of the Creative Commons Attribution 4.0 License (CC BY, <http://creativecommons.org/licenses/by/4.0/>), which permits unrestricted reuse of the work in any medium, provided the original work is properly cited. [DOI: 10.1149/2.0441907jss]



Manuscript submitted March 25, 2019; revised manuscript received June 11, 2019. Published June 24, 2019. *This paper is part of the JSS Focus Issue on Gallium Oxide Based Materials and Devices.*

The recent renewed interest in monoclinic  $\beta$ -Ga<sub>2</sub>O<sub>3</sub> arises from its potential for transparent optoelectronic devices up to UV due to its wide bandgap of  $\sim 4.9$  eV.<sup>1-6</sup> Furthermore, the large breakdown voltage of  $\sim 8$  MV cm<sup>-1</sup> is another property that makes this semiconductor a promising material for high power electronics.<sup>7</sup> Several studies have been published on other applications using this semiconductor putting in evidence the advantages of its particular properties, as for example in LEDs, large transparent and conductive substrates, intelligent windows, etc.<sup>3,8,9</sup> By controlling the stoichiometry<sup>10</sup> and by doping with Sn, Si, or Mg it is furthermore possible to control its conductivity.<sup>11-13</sup>

Two dimensional, high quality, flexible  $\beta$ -Ga<sub>2</sub>O<sub>3</sub> thin lamellas/membranes, produced from single crystals by mechanical exfoliation, demonstrated high potential for high power (opto) electronics,<sup>14</sup> as well as for mechanical applications such as microresonators.<sup>15</sup>

Thermal actuators are devices in which the mechanical movement results from the thermal lattice expansion due to Joule heating when a current passes the device.<sup>16</sup>  $\beta$ -Ga<sub>2</sub>O<sub>3</sub>, with a high thermal stability (melting point above 1700°C<sup>17</sup>) and low thermal conductivity, presents a relation ( $\alpha/k$ ) between the thermal expansion coefficient ( $\alpha$ ) and the thermal conductivity ( $k$ ) similar to the structural materials (metals and polysilicon<sup>16</sup>) conventionally used to design thermal actuators (see Table I which compares the relevant materials properties of several materials used in thermal actuators). In this context and considering that the relation ( $\alpha/k$ ) is among the most important parameters to evaluate the potential of an active material to design thermal actuators,<sup>18</sup> in this study flexible micro lamellas of  $\beta$ -Ga<sub>2</sub>O<sub>3</sub> are investigated.  $\beta$ -Ga<sub>2</sub>O<sub>3</sub> actuators are expected to be specially suited for applications in harsh temperature and radiation environments. The interest on electro-thermal actuators based on  $\beta$ -Ga<sub>2</sub>O<sub>3</sub> becomes even more relevant when additionally considering their optical properties, such as the high transparency in the UV and visible region as well as their waveguiding properties.<sup>19</sup>

Regarding the optical properties of  $\beta$ -Ga<sub>2</sub>O<sub>3</sub>, up to three different broad light emission bands have been revealed by luminescence studies with excitation above and below bandgap energy. These UV, blue and green bands, localized around 3.4, 3.0 and 2.4 eV, respectively, are assigned to different intrinsic defects in  $\beta$ -Ga<sub>2</sub>O<sub>3</sub>.<sup>10,20,21</sup> The UV band is being attributed to radiative recombination of free electrons with self-trapped holes or an exciton bound to an acceptor.<sup>21,22</sup> Concerning the blue band, it has been consensual that it is related with the oxygen vacancy concentration and, contrary to the UV band, this band can be observed under excitation below the bandgap energy. The blue band strongly depends on the sample preparation conditions and there are strong evidences that it is related with the electrical conductivity being only observed in conductive samples.<sup>20</sup> Binet et al.<sup>23</sup> estimated an activation energy for the deep trap involved in the UV and blue emission of  $\sim 0.3$  eV. Contrary to the UV and blue bands, the green band, localized at  $\sim 2.4$  eV, is usually attributed to impurities as for example Be, Ge and Sn.<sup>10,22</sup>

In this work, a systematic study is performed in a device based on a flexible  $\beta$ -Ga<sub>2</sub>O<sub>3</sub> lamella anchored at both extremes on a rigid substrate. The temperature of the device was calibrated with the help of Raman and PL measurements. A vertical movement of the actuator of up to 42.38  $\mu$ m, caused by thermal expansion, was observed and evidences the potential of this material for thermal actuators.

### Experimental

Thin and flexible lamellas of  $\beta$ -Ga<sub>2</sub>O<sub>3</sub>, with dimensions of some mm length with a thickness lower than 10  $\mu$ m with a (100) surface orientation were mechanically exfoliated from  $\beta$ -Ga<sub>2</sub>O<sub>3</sub> bulk crystals grown using the floating zone technique as described in Ref. 9. The mechanical exfoliation process using a thermal-release tape (REVAL-PHA) was done following the procedure described in Ref. 30. The thin lamellas of Ga<sub>2</sub>O<sub>3</sub> were transferred to a silicon wafer with a silicon oxide layer of 2  $\mu$ m thickness that works as an electrical isolating layer.

<sup>z</sup>E-mail: [marcoperes@ctn.tecnico.ulisboa.pt](mailto:marcoperes@ctn.tecnico.ulisboa.pt)

**Table I.** Comparison of different physical parameters for different materials used for thermal actuators.<sup>18,24-29</sup>

Material	Bandgap (eV)	Young Modulus (GPa)	Lattice thermal expansion coefficient $\alpha$ ( $\times 10^{-6} \text{K}^{-1}$ )	Thermal conductivity $k$ ( $\text{Wm}^{-1} \text{K}^{-1}$ )	Relation $\alpha/k$ ( $\times 10^{-6} \text{Wm}^{-1}$ )
Al	—	69	23	155	0.15
Ni	—	210	12.7	83	0.15
SiO <sub>2</sub>	5	150	0.4	2	0.2
Diamond	5.47	1050	1.6	2200	$7.2\text{E}^{-4}$
$\beta$ -Ga <sub>2</sub> O <sub>3</sub>	4.9	230	3.37-4.2	23	0.14-0.2

Two lateral Au/Al contacts with a thickness of 100 nm and 200 nm, with a separation of about 1.5 mm were deposited on the surface of the  $\beta$ -Ga<sub>2</sub>O<sub>3</sub> lamellas by RF-sputtering at room temperature, the size and position of the contacts were defined using a hard mask. Two anchors were created by two pads of indium positioned on top of the two contacts and melted using a hot plate at 200°C during five minutes. These two pads work also as electrical contacts.

In Figure 1a a schematic of this type of device is shown where the relative directions of the three main crystalline axes ( $a$ ,  $b$  and  $c$ ) of the  $\beta$ -Ga<sub>2</sub>O<sub>3</sub> lamella are indicated. The objective of these two anchors is to fix the two extremities of the lamella and force a vertical movement when a thermal expansion of the lamella takes place induced by self-heating when an electrical current passes through it. The deflection (vertical movement  $Z'$ - $Z$  (see Figure 1a)) due to the thermal expansion of this kind of devices is given by the simple relation:

$$\text{Deflection} = [L^2 + 2L\Delta L + \Delta L^2 - L^2\cos(\theta)^2]^{1/2} - L\sin(\theta) \quad [1]$$

where  $\theta$  is the initial deflection angle when the device is unbiased,  $L$  is approximately half of the lamella length for small  $\theta$  and  $\Delta L = L\alpha\Delta T$  is the elongation due to the thermal expansion with,  $\alpha$  the thermal expansion coefficient and  $\Delta T$  the temperature variation associated to the Joule effect. Figure 1b shows an optical microscopy image of the studied device, with a dimension of  $1500 \times 600 \mu\text{m}^2$  and a thickness of  $\sim 5 \mu\text{m}$  (the thickness was estimated by Rutherford Backscattering spectrometry as described in Ref. 31).

The optical characterization was performed by photoluminescence and micro-Raman spectroscopy. The photoluminescence (PL) spectra in the range between 200 nm and 800 nm were acquired using a CCD camera (JY Symphony) coupled to a monochromator with a diffraction grating of 1200 lines/mm (Triax 150 JY). As excitation source,

a 240 nm LED (UVTOP 240) was used working with a power of  $50 \mu\text{W}$  and a spot size of  $4 \times 4 \text{mm}^2$ . The PL is collected and guided to the monochromator through an optical fiber with a core of  $600 \mu\text{m}$  diameter. The presented spectra were corrected to the optical response of the PL system.

The micro-Raman analysis was conducted in backscattering configuration on a Jobin Yvon HR800 instrument (Horiba, Japan), using a 600 lines/mm grating and the 441.6 nm laser line of a HeCd laser (Kimmon IK Series, Japan). The excitation laser line was suppressed by a pair of edge filters placed in series, allowing Raman acquisition starting at  $50 \text{cm}^{-1}$ . A 50x objective (spot size  $\sim 2$  microns, numeric aperture = 0.9, Olympus, Japan) was used to focus the laser light onto the sample and to collect the Raman radiation in a backscattering configuration and further direct the light to the spectrometer equipped with a Peltier cooled (223 K) back-thinned CCD detector. The apparatus was operated in the confocal mode, setting the iris to 0.25 mm and the acquisition time to 2 s with 3 accumulations. All the results presented in this paper using these different techniques were obtained in air.

A non-contact 3D optical profiler (S neox 3D, Sensofar) was used to measure the thickness and the deflection of the lamellas as a function of the applied current. This optical profiler is equipped with a black and white  $1360 \times 1024$  pixels CCD sensor that, when combined with a display of  $2560 \times 1440$  pixels, yields high resolution optical images. The vertical resolution in this equipment is further enhanced by a piezo assisted Z-axis deflection movement (limited to  $200 \mu\text{m}$ ) without any further mechanical components. The confocal mode was used to measure the deflection of the  $\beta$ -Ga<sub>2</sub>O<sub>3</sub> lamellas as a function of the applied current. This mode used an objective with 10x magnification and a numerical aperture (NA) of 0.30 having an optical resolution in

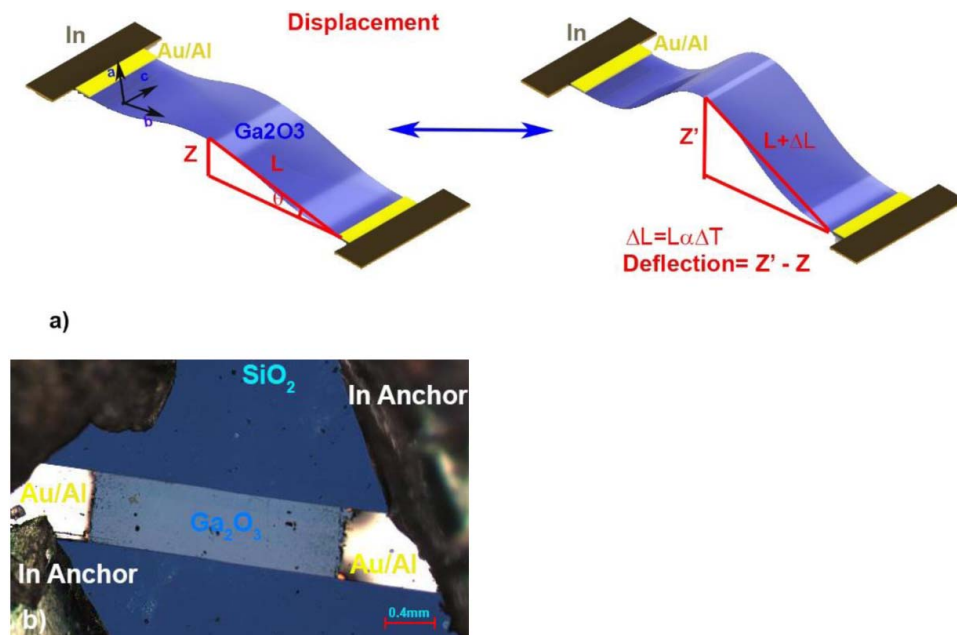


**Figure 1.** a) Conceptual view of the thermal actuator device. b) Microscopy image of the thermal actuator based on micro-lamellas of Ga<sub>2</sub>O<sub>3</sub>.

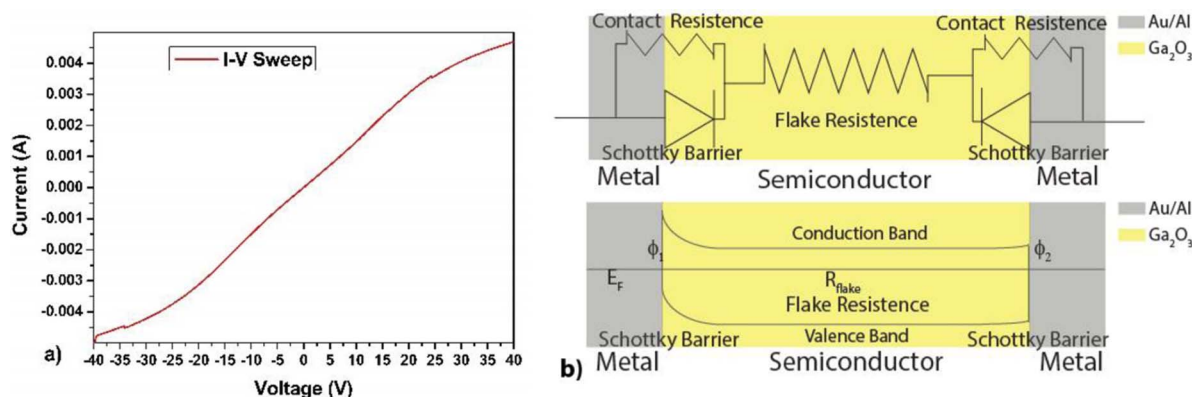


**Figure 2.** a) I-V curve of the thermal actuator device. b) Schematic of the equivalent electric circuit adapted from Ref. 32, where  $E_F$ ,  $\Phi_1$ ,  $\Phi_2$  correspond to the Fermi level and the Schottky barrier heights.

XY of  $0.46 \mu\text{m}$  and a vertical resolution (Z) of  $25 \text{ nm}$ , for a visualization area of  $1754 \times 1320 \mu\text{m}^2$ . In order to measure the thickness of the entire micro-lamella with better accuracy, interferometric analysis in Vertical Shift Interferometric (VSI) mode was used. In this case, a  $10\times$  objective was also used and it provides optical (XY) and vertical (Z) resolutions around  $0.50 \mu\text{m}$  and  $1 \text{ nm}$ , respectively.

The electrical characterization was performed using a semiconductor device analyzer (AGILENT B1500). All the electrical characterization was performed at room temperature.

## Results and Discussion

Figure 2a shows the obtained I-V curve of this device where the metal-semiconductor-metal configuration can be described by the equivalent circuit presented in Figure 2b composed of two back-to-back polarized Schottky diodes separated by a resistance. The almost linear and symmetric curve observed in this particular device suggests that the contacts are almost ohmic. However, I-V curves of other devices prepared in a similar way showed nonlinear and even asymmetrical curves.<sup>31</sup> This evidence suggests that heterogeneous distribution of interface defects, intrinsic and extrinsic, such as defects on the surface of the  $\beta\text{-Ga}_2\text{O}_3$  lamellas resultant from the exfoliation process, probably plays a major role in the electrical behavior. Despite these challenges in fabricating devices with reproducible electrical properties, it should be noted that all these devices exhibited similar properties in terms of self-heating and thermal expansion.

In order to assess the thermal expansion of the actuator, it was first necessary to establish the calibration of the beam temperature as a function of the applied electrical power (note that this calibration may be different for different devices due to the varying size of exfoliated crystals and due to the above mentioned variations in contact properties). For this, temperature and power dependent Raman and PL measurements were performed on the same device. Figure 3a shows the  $\mu\text{-Raman}$  spectra of a bulk  $\beta\text{-Ga}_2\text{O}_3$  crystal taken at temperatures from RT to 798 K where the sample temperature was adjusted using a heatable sample stage. Figure 3b shows  $\mu\text{-Raman}$  spectra as a function of the applied power (without external heating), measured in the middle of the lamella between the two electrodes. For each measurement, the focal distance was realigned to maximize the Raman signal in order to compensate the defocussing caused by the vertical movement of the crystal as the power is increased. The intense and sharp Raman peaks (similar to those of the bulk  $\beta\text{-Ga}_2\text{O}_3$  crystal) confirm the good structural quality of the exfoliated micro-lamellas obtained by mechanical exfoliation. Due to the limitations of the spectral resolution and due to the superposition with two strong bands of the silicon substrate, in these spectra only 8 peaks (from the 15 predicted by group theory and previously observed<sup>33</sup>) associated to the  $A_g$  and  $B_g$  modes of  $\beta\text{-Ga}_2\text{O}_3$  were identified. In agreement with Doynng et al. and Rao R. et al.,<sup>34,35</sup> these 8 peaks can be classified in three main groups: the high-frequency group associated to the stretching and bending of the

$\text{GaO}_4$  tetrahedra ( $770\text{-}500 \text{ cm}^{-1}$ ), the mid-frequency group associated to the deformation of the  $\text{Ga}_2\text{O}_6$  octahedra ( $480\text{-}310 \text{ cm}^{-1}$ ) and the low-frequency group associated to the liberation and translation of the tetrahedral-octahedra chains (below  $200 \text{ cm}^{-1}$ ). Comparing both Raman studies, it is observed that the peaks shift to lower wavenumbers both for higher applied powers and higher temperatures. Figure 3c plots the Raman peak position of the  $B_g^3$  and  $A_g^{10}$  modes as a function of the temperature extracted from the spectra in Fig. 3a. These two modes were chosen for being the most intense peaks and for being sensitive to the stretching and bending of the  $\text{GaO}_4$  tetrahedral and to the deformation of the  $\text{Ga}_2\text{O}_6$  octahedra in agreement with.<sup>35</sup>

The dependence of the peak shift with the temperature of the different Raman modes is well described by the empirical Cui formula:<sup>36</sup>

$$\omega(T) = \omega_0 - \frac{A}{e^{\frac{Bhc\omega_0}{k_B T}} - 1} \quad [2]$$

where  $A$  and  $B$  are fitting parameters,  $\omega_0$  is the Raman phonon wavenumber at 0 K and  $k_B$  is the Boltzmann constant,  $h$  the Planck constant and  $c$  the speed of light in vacuum. The temperature dependences of both  $A_g^{10}$  and  $B_g^3$  modes are well fitted by expression 2 (see Figure 3c); this fact suggests that the effects of bending induced by the Joule-heating (responsible for the vertical movement) play a minor role on the Raman shift suggesting that the temperature should be the main responsible for the observed Raman shifts. Rewriting expression 2 by solving it for  $T$  and using the fitted parameters ( $A, B$  and  $\omega_0$ ), a calibration curve of the expected temperature for a certain applied power can be determined. Figure 3d shows the determined temperature as a function of the applied power considering the wavenumbers of both Raman modes ( $B_g^3$  and  $A_g^{10}$ ) in the spectra shown in Figure 3b.

As an independent confirmation of the temperature calibration as well as to understand the effects of the temperature on the luminescence properties of the exfoliated lamellas, a PL study as a function of the temperature was performed in a similar lamella used to fabricate the thermal device, but not anchored to the substrate in order to avoid any strain induced by the lamella bending. The PL spectra are dominated by an asymmetric broad band with a maximum at  $\sim 3.0 \text{ eV}$  (see Figure 4a). The dependence on the temperature is characterized by a strong quenching without any energy shift. Comparing to different reported works,<sup>20,23,37</sup> this asymmetric band is assigned to an overlap of the two emission bands, UV and blue, located at  $\sim 3.4 \text{ eV}$  and  $3.0 \text{ eV}$ , respectively. Based on the Urbach law, Binet et al. estimated an activation energy of  $0.3 \text{ eV}$  for the thermal quenching of the blue band and associated this band to a deep acceptor level  $0.3 \text{ eV}$  above the valence band maximum.<sup>23</sup> The UV band, on the other hand, was associated to self-trapped excitons supported by recent computational results.<sup>38</sup> Electron paramagnetic resonance studies estimated an activation energy of about  $0.19 \text{ eV}$  for this process.<sup>39</sup> In this study, we adopt the activation energy estimated by Binet et al. for the blue band, although the underlying process is still under debate since density functional

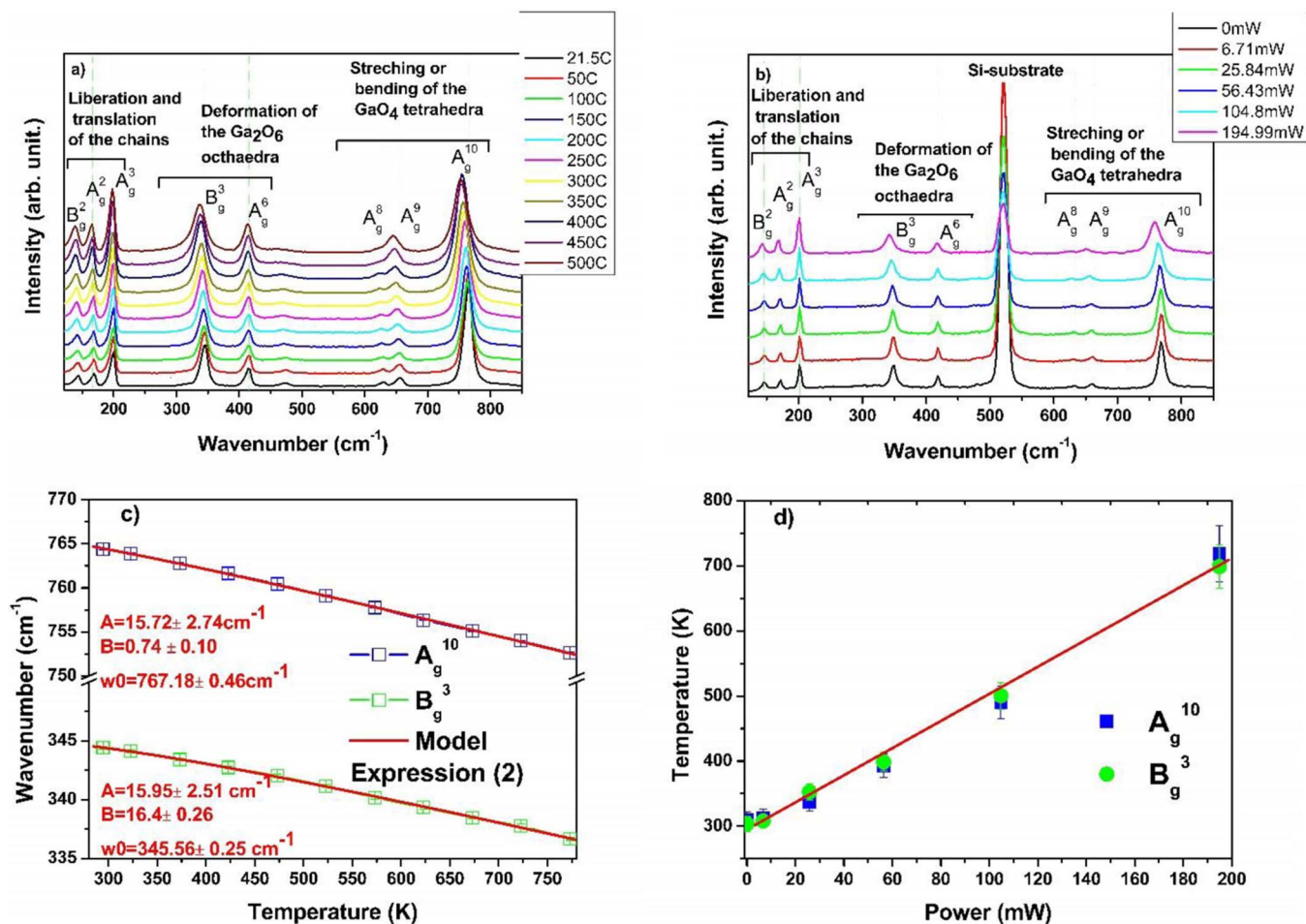


**Figure 3.** a) Temperature dependent Raman spectra of a  $\text{Ga}_2\text{O}_3$  single crystal. b) Power dependent Raman spectra of the thermal actuator device. c) Raman peak shift of the  $\text{B}_g^3$  and  $\text{A}_g^{10}$  modes as a function of the temperature extracted from the spectra in a) and fit of the experimental data using Equation 2. d) Temperature-power calibration curve determined from the peak positions of the  $\text{B}_g^3$  and  $\text{A}_g^{10}$  modes extracted from b), the red line is a guide for the eye.

simulations point to typical acceptor levels above 1.3 eV in  $\text{Ga}_2\text{O}_3$ .<sup>40</sup> Indeed, the dependence of the integrated PL intensity measured (i.e. englobing both bands) is well fitted (see Figure 4c) assuming an activation energy of 0.3 eV, using the conventional law for the thermal quenching<sup>41</sup> described by:

$$I(T) = \frac{I_0}{1 + A \exp(-E_a/k_B T)} \quad [3]$$

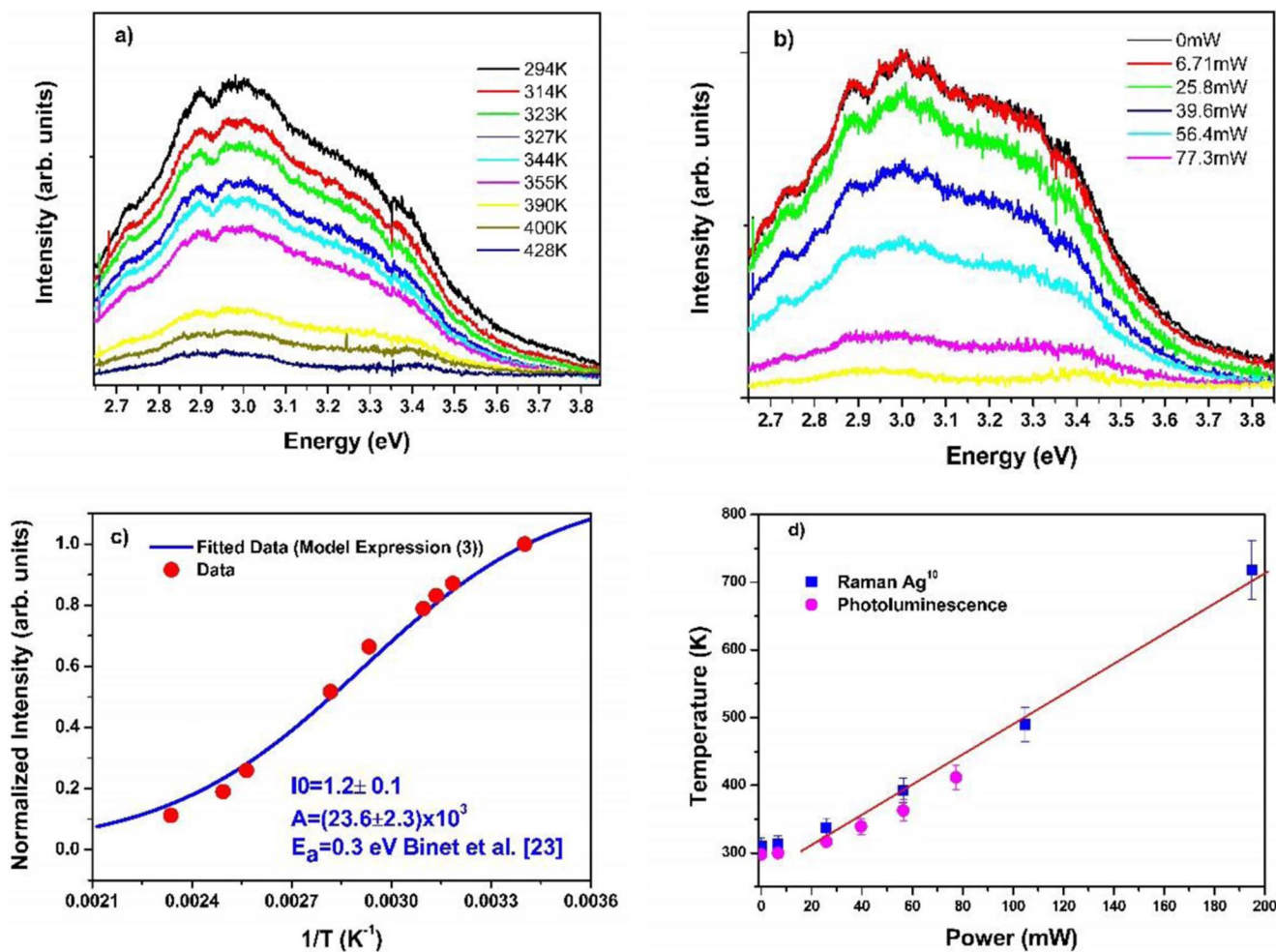
where  $I_0$  is the intensity at 0 K,  $A$  is a constant describing the relation between radiative and non-radiative recombination lifetimes and  $E_a$  is the activation energy.

Figure 4b shows the PL spectra as a function of the applied power. The differences in the shape of the spectra compared with the study with the temperature are due to different interference effects that occur due to the different collection angles.<sup>42</sup> Effectively, because the  $\text{Ga}_2\text{O}_3$  lamellas are very small and thin, with our PL setup it is difficult to keep the same collection conditions (namely the collection angle) used for the temperature study. As performed in the Raman study, in order to avoid the influence of changes on the collection zone due to the vertical movement, for each spectrum acquired at different power the PL signal was maximized.

Similar to the temperature dependent results, the PL intensity quenches for higher applied power (increased Joule heating) without changes in the line shape; for powers above 100 mW the quenching is almost complete. Rewriting Equation 3 in order to have an expression for  $T$  as function of the normalized integrated intensity ( $I/I_0$ ), the temperature of the flake resultant from the self-heating for each of the power dependent spectra was estimated. As shown in Figure 4d,

following this methodology, the estimated temperatures are in excellent agreement with the estimates based on the Raman study. These self-consistent results confirm that, on the one hand, the Raman peak positions are not strongly influenced by the bending of the crystal and that, on the other hand, the luminescence quenching of intrinsic defect luminescence can be used as a tool to calibrate the temperature of the beam as a function of the applied power. It is worth mentioning that similar luminescence quenching behavior was observed when a current was applied during cathodoluminescence and ionoluminescence measurements for more than 250 cycles (not shown) suggesting that this effect is stable and reproducible.

In order to characterize the mechanical movement of the device, the vertical displacement and deformation of the  $\text{Ga}_2\text{O}_3$  lamella as a function of the applied power was measured using an optical profiler. Examples are presented in Figures 5a and 5b showing the optical images of the unbiased device and after applying a power of 194.9 mW ( $I = 5$  mA and  $V = 38.98$  V), respectively. A buckling of the lamella is clearly observed when applying dc currents from 0 to 5 mA to the device with a vertical elevation of more than 40  $\mu\text{m}$  for the highest tested current. From the optical images the buckling profiles of the micro-lamella were extracted and are plotted in Figure 5c. From this figure is possible to confirm that the center of the profile as function of the dc current keeps almost constant as expected for this kind of device. From these profiles, the length of the beam parallel to the  $b$  axis as a function of the applied power was calculated by integration (see Figure 5d). This figure shows that the evolution of the beam length between the two contacts is almost linear, namely, in the region of higher applied power. The non-linearity for low powers can be justified



**Figure 4.** a, b) evolution of the photoluminescence of the device as a function of the temperature and applied power, respectively. c) Integrated and normalized PL intensity as function of the temperature. The blue line represents the fit using Equation 3. d) Estimated temperature as a function of the power, derived from the photoluminescence intensity in b). For comparison, the calibration curve obtained from Raman (Fig. 3d) was also included in the graph. The red line is a guide to the eye.

considering that when the vertical displacement starts the thermal contact to the substrate decreases significantly. For high power, the air becomes the main channel of thermal losses because most of the lamella loses direct contact to the substrate. This is supported by the fact that the heat transfer coefficient ( $h$ ) of air is considerably lower than that of the  $\text{SiO}_2/\text{Si}$  substrate.<sup>43</sup>

Considering that  $\beta\text{-Ga}_2\text{O}_3$  has a center of symmetry, no piezoelectric effects are expected<sup>8,17</sup> which means that the effect reported here should be purely thermal. Indeed, Figure 5d compares the beam length as a function of the applied power with the theoretical beam length estimated considering the lattice thermal expansion of  $\beta\text{-Ga}_2\text{O}_3$  along the  $b$  axis being described by  $\alpha = 4.2 \times 10^{-6} \text{ K}^{-1}$ <sup>24</sup> using the standard definition for the linear thermal expansion  $\Delta L = L \times \alpha_a \times \Delta T$ . Figure 5d shows that the elongation estimated by the expression for the linear thermal expansion fits very well the tendency of the elongation measured as a function of the applied power/temperature. This result corroborates that all the mechanical movement is effectively due to a thermal expansion.

### Conclusions

A thermal actuator based on a flexible lamella of  $\beta\text{-Ga}_2\text{O}_3$  anchored to the substrate at the two extremes was designed and successfully tested. When a current is applied to the  $\beta\text{-Ga}_2\text{O}_3$  lamella, an elongation occurs along the  $b$  axis of the crystal due to thermal lattice expansion resulting in a buckling of the lamella and thus a ver-

tical movement. These results reveal the potential of  $\beta\text{-Ga}_2\text{O}_3$  micro-lamellas/membranes for electro-thermal actuators. The Joule-heating responsible for the elongation affects also the optical emission, namely the emission intensity of the UV and blue bands. The thermal quenching of these emission bands allows calibrating the temperature of the  $\beta\text{-Ga}_2\text{O}_3$  lamella.  $\mu$ -Raman results corroborate the Joule-heating effect responsible for the luminescence quenching. Furthermore, the good agreement between calibration curves derived from PL and Raman studies demonstrates that the effect of strain due to bending on the Raman spectra is insignificant.

This work demonstrates that combining the thermal, optical and electrical properties of flexible micro-lamellas or membranes of  $\beta\text{-Ga}_2\text{O}_3$ , this material can be considered for the design of new kinds of micro-opto-electro-mechanical (MOEMs) devices such as camera focus systems, micro-mirrors and optical and microwave couplers. On the other hand, the results presented in this paper demonstrate also the potential of  $\beta\text{-Ga}_2\text{O}_3$  in devices where the self-heating processes could play an important role, such as for example in-situ damage recovery of detectors for ionizing radiation or for the recovery of aging effects in electronic devices.

### Acknowledgments

This work was supported by the Portuguese Foundation for Science and Technology (FCT), under the projects UID/FIS/50010/2019 and PTDC/CTM-CTM/28011/2017, LISBOA-01-0145-FEDER-028011.

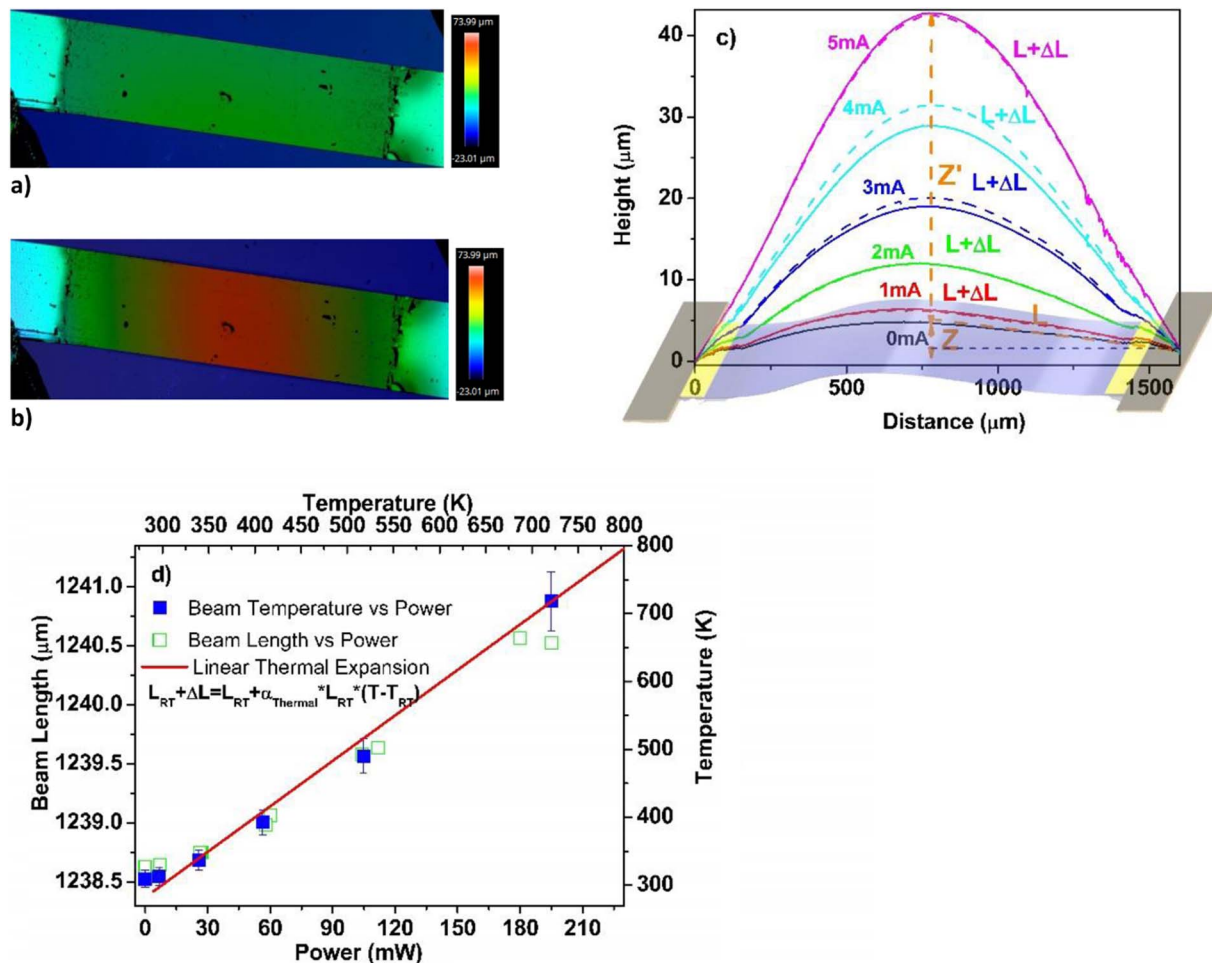


**Figure 5.** Confocal images of the lamella a) unbiased and b) biased with a dc current of 5 mA. c) Profiles of the lamella biased with different dc currents with positive voltage (solid line) and negative voltage (dashed line). d) Beam length as function of power and temperature where the latter was estimated from Raman and PL using Equations 2 and 3, respectively. The calculated linear thermal expansion (red line) as function of the temperature was also included.

## ORCID

Marco Peres <https://orcid.org/0000-0001-6774-8492>

## References

1. K. Takakura, D. Koga, H. Ohya, J. M. Rafi, Y. Kayamoto, M. Shibuya, H. Yamamoto, and J. Vanhellefont, "Evaluation of the crystalline quality of  $\beta$ -Ga<sub>2</sub>O<sub>3</sub> films by optical absorption measurements" *Phys. B Condens. Matter*, **404**, 4854 (2009).
2. H. Tippins, "Optical Absorption and Photoconductivity in the Band Edge of  $\beta$ -Ga<sub>2</sub>O<sub>3</sub>" *Phys. Rev.*, **140**, A316 (1965).
3. M. M. Muhammed, M. Peres, Y. Yamashita, Y. Morishima, S. Sato, N. Franco, K. Lorenz, A. Kuramata, and I. S. Roqan, "High optical and structural quality of GaN epilayers grown on (201)  $\beta$ -Ga<sub>2</sub>O<sub>3</sub>" *Appl. Phys. Lett.*, **105**, 042112 (2014).
4. M. Mohamed, C. Janowitz, I. Unger, R. Manzke, Z. Galazka, R. Uecker, R. Fornari, J. R. Weber, J. B. Varley, and C. G. Van De Walle, "The electronic structure of  $\beta$ -Ga<sub>2</sub>O<sub>3</sub>" *Appl. Phys. Lett.*, **97**, 2008 (2010).
5. S. J. Pearton, J. Yang, P. H. Cary IV, F. Ren, J. Kim, M. J. Tadjer, and M. A. Mastro, "A review of Ga<sub>2</sub>O<sub>3</sub> materials, processing, and devices" *Appl. Phys. Rev.*, **5**, 011301 (2018).
6. M. Higashiwaki and G. H. Jessen, "Guest Editorial: The dawn of gallium oxide microelectronics Guest Editorial: The dawn of gallium oxide microelectronics" *Appl. Phys. Lett.*, **112**, 060401 (2018).
7. M. Higashiwaki, K. Sasaki, A. Kuramata, T. Masui, and S. Yamakoshi, "Development of gallium oxide power devices" *Phys. Status Solidi Appl. Mater. Sci.*, **211**, 21 (2014).
8. E. G. Villora, S. Arjoca, K. Shimamura, D. Inomata, and K. Aoki, " $\beta$ -Ga<sub>2</sub>O<sub>3</sub> and single-crystal phosphors for high-brightness white LEDs and LDs, and  $\beta$ -Ga<sub>2</sub>O<sub>3</sub> potential for next generation of power devices" *Proc. SPIE*, **8987**, 89871U (2014).
9. E. G. Villora, K. Shimamura, Y. Yoshikawa, K. Aoki, and N. Ichinose, "Large-size  $\beta$ -Ga<sub>2</sub>O<sub>3</sub> single crystals and wafers" *J. Cryst. Growth*, **270**, 420 (2004).
10. L. Binet and D. Gourier, "Origin of the blue luminescence of  $\beta$ -Ga<sub>2</sub>O<sub>3</sub>" *J. Phys. Chem. Solids*, **59**, 1241 (1998).
11. N. Suzuki, S. Ohira, M. Tanaka, T. Sugawara, K. Nakajima, and T. Shishido, "Fabrication and characterization of transparent conductive Sn-doped  $\beta$ -Ga<sub>2</sub>O<sub>3</sub> single crystal" *Physica Status Solidi (C) Current Topics in Solid State Physics*, **4**, 2310 (2007).
12. T. Onuma, S. Fujioka, T. Yamaguchi, M. Higashiwaki, K. Sasaki, T. Masui, and T. Honda, "Correlation between blue luminescence intensity and resistivity in  $\beta$ -Ga<sub>2</sub>O<sub>3</sub> single crystals" *Appl. Phys. Lett.*, **103**, 041910 (2013).
13. Z. Galazka, K. Irscher, R. Uecker, R. Bertram, M. Pietsch, A. Kwasniewski, M. Naumann, T. Schulz, R. Schewski, D. Klimm, and M. Bickermann, "On the bulk  $\beta$ -Ga<sub>2</sub>O<sub>3</sub> single crystals grown by the Czochralski method" *J. Cryst. Growth*, **404**, 184 (2014).
14. J. Kim, M. A. Mastro, M. J. Tadjer, and J. Kim, "Quasi-Two-Dimensional h-BN/ $\beta$ -Ga<sub>2</sub>O<sub>3</sub> Heterostructure Metal-Insulator-Semiconductor Field-Effect Transistor" *ACS Appl. Mater. Interfaces*, **9**, 21322 (2017).
15. X.-Q. Zheng, J. Lee, S. Rafique, L. Han, C. A. Zorman, H. Zhao, and P. X.-L. Feng, "Ultrawide Band Gap  $\beta$ -Ga<sub>2</sub>O<sub>3</sub> Nanomechanical Resonators with Spatially Visualized Multimode Motion" *ACS Appl. Mater. Interfaces*, **9**, 43090 (2017).
16. L. Que, J. S. Park, and Y. B. Gianchandani, "Bent-beam electrothermal actuators-Part I: Single beam and cascaded devices" *J. Microelectromechanical Syst.*, **10**, 247 (2001).
17. A. E. Romanov, S. I. Stepanov, V. I. Nikolaev, and V. E. Bougrov, "Gallium Oxide: Properties and Applications - A Review" *Rev. Adv. Mater. Sci.*, **44**, 63 (2016).
18. J. K. Luo, A. J. Flewitt, S. M. Spearing, N. A. Fleck, and W. I. Milne, "Modelling and fabrication of microsprings thermal actuator" **1**, 355 (2004).
19. E. Nogales, J. A. García, B. Meñéndez, and J. Piqueras, "Red luminescence of Cr in  $\beta$ -Ga<sub>2</sub>O<sub>3</sub> nanowires" *J. Appl. Phys.*, **101**, 033517 (2007).

20. T. Onuma, S. Fujioka, T. Yamaguchi, M. Higashiwaki, K. Sasaki, T. Masui, and T. Honda, "Correlation between blue luminescence intensity and resistivity in  $\beta$ -Ga<sub>2</sub>O<sub>3</sub> single crystals" *Appl. Phys. Lett.*, **103**, 041910 (2013).
21. T. Harwig, F. Kellendonk, and S. Slappendel, "The ultraviolet luminescence of  $\beta$ -galliumsesquioxide" *J. Phys. Chem. Solids*, **39**, 675 (1978).
22. E. G. Villora, T. Atou, T. Sekiguchi, T. Sugawara, M. Kikuchi, and T. Fukuda, "Cathodoluminescence of undoped  $\beta$ -Ga<sub>2</sub>O<sub>3</sub> single crystals" *Solid State Commun.* **120**, 455 (2001).
23. L. Binet and D. Gourier, "Origin of the blue luminescence of  $\beta$ -Ga<sub>2</sub>O<sub>3</sub>" *J. Phys. Chem. Solids*, **59**, 1241 (1998).
24. F. Orlandi, F. Mezzadri, G. Calestani, F. Boschi, and R. Fornari, "Thermal expansion coefficients of  $\beta$ -Ga<sub>2</sub>O<sub>3</sub> single crystals" *Appl. Phys. Express*, **8**, 8 (2015).
25. M. Handweg, R. Mitdank, Z. Galazka, and S. F. Fischer, "Temperature-dependent thermal conductivity and diffusivity of a Mg-doped insulating  $\beta$ -Ga<sub>2</sub>O<sub>3</sub> single crystal along [100], [010] and [001]" *Semicond. Sci. Technol.*, **31**, 125006 (2016).
26. A. J. Flewitt, J. Luo, W. I. Milne, D. F. Moore, N. A. Fleck, J. H. He, and S. M. Spearing, "Development of an all-metal electrothermal actuator and its applications" *Proc. SPIE 5344, MEMS/MOEMS Components and Their Applications* (2004).
27. T. Sato, K. Ohashi, T. Sudoh, K. Haruna, and H. Maeta, "Thermal expansion of a high purity synthetic diamond single crystal at low temperatures" *Phys. Rev. B*, **65**, (2002).
28. C. A. Klein and G. F. Cardinale, "Young's modulus and Poisson's ratio of CVD diamond" *Diam. Relat. Mater.*, **2**, 918 (1993).
29. D. J. Twitchen, C. S. J. Pickles, S. E. Coe, R. S. Sussmann, and C. E. Hall, "Thermal conductivity measurements on CVD diamond" *Diam. Relat. Mater.*, **10**, 731 (2001).
30. R. Mitdank, S. Dusari, C. Bülow, M. Albrecht, Z. Galazka, and S. F. Fischer, "Temperature-dependent electrical characterization of exfoliated  $\beta$ -Ga<sub>2</sub>O<sub>3</sub> micro flakes" *Phys. Status Solidi*, **211**, 543 (2014).
31. M. Peres, L. C. Alves, F. Rocha, N. Catarino, C. Cruz, E. Alves, A. G. Silva, E. G. Villora, K. Shimamura, and K. Lorenz, "In Situ Characterization and Modification of  $\beta$ -Ga<sub>2</sub>O<sub>3</sub> Flakes Using an Ion Micro-Probe" *Phys. Status Solidi*, **1800190**, 1 (2018).
32. A. J. Chiquito, C. A. Amorim, O. M. Berengue, L. S. Araujo, E. P. Bernardo, and E. R. Leite, "Back-to-back Schottky diodes: The generalization of the diode theory in analysis and extraction of electrical parameters of nanodevices" *J. Phys. Condens. Matter*, **24**, 225303 (2012).
33. C. Kranert, C. Sturm, R. Schmidt-Grund, and M. Grundmann, "Raman tensor elements of  $\beta$ -Ga<sub>2</sub>O<sub>3</sub>" *Sci. Rep.*, **6**, 35964 (2016).
34. R. Rao, A. M. Rao, B. Xu, J. Dong, S. Sharma, and M. K. Sunkara, "Blueshifted Raman scattering and its correlation with the [110] growth direction in gallium oxide nanowires" *J. Appl. Phys.*, **98**, (2005).
35. D. Dohy, G. Lucazeau, and A. Revcolevschi, "Raman spectra and valence force field of single-crystalline  $\beta$ -Ga<sub>2</sub>O<sub>3</sub>" *J. Solid State Chem.*, **45**, 180 (1982).
36. J. B. Cui, K. Amtmann, J. Ristein, and L. Ley, "Noncontact temperature measurements of diamond by Raman scattering spectroscopy" *J. Appl. Phys.*, **83**, 7929 (1998).
37. E. G. Villora, K. Hatanaka, H. Odaka, T. Sugawara, T. Miura, H. Fukumura, and T. Fukuda, "Luminescence of undoped  $\beta$ -Ga<sub>2</sub>O<sub>3</sub> single crystals excited by picosecond X-ray and sub-picosecond UV pulses" *Solid State Commun.* **127**, 385 (2003).
38. J. B. Varley, A. Janotti, C. Franchini, and C. G. Van De Walle, "Role of self-trapping in luminescence and p-type conductivity of wide-band-gap oxides" *Phys. Rev. B - Condens. Matter Mater. Phys.*, **85**, 2 (2012).
39. B. E. Kananen, N. C. Giles, L. E. Halliburton, G. K. Foundos, K. B. Chang, and K. T. Stevens, "Self-trapped holes in  $\beta$ -Ga<sub>2</sub>O<sub>3</sub> crystals" *J. Appl. Phys.*, **122**, (2017).
40. J. L. Lyons, "A survey of acceptor dopants for  $\beta$ -Ga<sub>2</sub>O<sub>3</sub>" *Semicond. Sci. Technol.*, **33**, 05LT02 (2018).
41. M. Leroux, N. Grandjean, B. Beaumont, G. Nataf, F. Semond, J. Massies, and P. G. "Temperature quenching of photoluminescence intensities in undoped and doped GaN" *J. Appl. Phys.*, **86**, 3721 (1999).
42. J. K. Larsen, S. Y. Li, J. J. S. Scragg, Y. Ren, C. Hägglund, M. D. Heinemann, S. Kretzschmar, T. Unold, and C. Platzer-Björkman, "Interference effects in photoluminescence spectra of Cu<sub>2</sub>ZnSnS<sub>4</sub> and Cu(In,Ga)Se<sub>2</sub> thin films" *J. Appl. Phys.*, **118**, (2015).
43. H. Zhou, K. Maize, J. Noh, A. Shakouri, and P. D. Ye, "Thermodynamic Studies of  $\beta$ -Ga<sub>2</sub>O<sub>3</sub> Nanomembrane Field-Effect Transistors on a Sapphire Substrate" *ACS Omega*, **2**, 7723 (2017).